University of Bristol - Explore Bristol Research
General rights

RMetS

Royal Meteorological Society
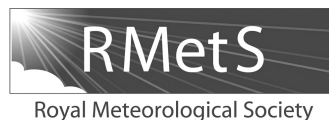
Offshore wind turbine clutter characteristics and identification in operational C-band weather radar measurements

Will Hall,[a]* Miguel A. Rico-Ramirez[a] and Stefan Krämer[b]

[a]*Department of Civil Engineering, University of Bristol, Bristol, UK*
[b]*Institute for Technical and Scientific Hydrology Ltd., Hanover, Germany*

Correspondence to: W. Hall, 93 Woodland Road, University of Bristol, Bristol, BS8 1US, UK. E-mail: w.hall@bristol.ac.uk

The aim of this work is to update ground-clutter classification methods in weather radar rainfall measurements to more accurately identify clutter pixels from wind farms. Measurements from two dual-polarised weather radars, based in the United Kingdom, will be used to determine the characteristics of multiple wind farms in the North Sea and the Irish Sea. Currently 21 of the top 25 largest offshore wind farms are located in these regions. The extensive area occupied by the wind farms creates problems for weather radars located in the neighbouring European countries. Datasets of wind-farm, precipitation and ground-clutter pixels were aggregated from Thurnham Radar measurements to form novel membership functions that can be used in a fuzzy logic classification system to identify wind-farm clutter. When only ground-clutter datasets were used for classification, areas of the radar scans taken up by wind-farm clutter were misclassified as rainfall. The inclusion of wind-farm measurements led to an increase in the ability of the algorithm to detect these pixels as clutter, as the Heidke Skill Score increased from 67.4 to 97.8%. However there was a slight increase in the number of precipitation pixels incorrectly classified as clutter, with the false alarm rate increasing from 0.05 to 1.24% when all variables are used. The algorithm performed slightly better when applied to another radar on Hameldon Hill, showing promise for application to the UK network without recalibration of membership functions.

Key Words: polarimetric radar; weather radar; wind farm; wind turbine; clutter; C-band

Received 18 April 2016; Revised 30 October 2016; Accepted 2 November 2016; Published online in Wiley Online Library

1. Introduction

The North Sea contains two of the top three largest wind farms worldwide, called the London Array and Greater Gabbard. The North Sea is a major area for offshore wind power with Germany, The Netherlands, and the United Kingdom all planning and commissioning new projects in the following years. Turbines within these offshore farms reach heights of 150 m including the blades and motor hub. These can cause substantial problems to weather radars due to backscatter effects from the radar main beam and side lobes leading to the appearance of non-meteorological echoes also known as clutter (Harrison, 2012). This effect is compounded by the vast size of the farms with the London Array having an area of $100 \, \text{km}^2$ leading to the contamination of over 200 pixels ($1°$ by 600 m size) in scans from the nearest weather radar, located in Thurnham, near London, United Kingdom. World Meteorological Organisation (WMO) guidelines state that beyond 45 km wind turbines are generally not observed, though this is no longer the case with the subsequent building of large offshore wind farms (WMO, 2005, 2010).

Many simulations of the potential impacts of wind turbines and farms have been performed using various methods (Hood *et al.*,

2010; Gallardo-Hernando *et al.*, 2011; Angulo Pita *et al.*, 2015). Gallardo-Hernando *et al.* (2011) studied the effect of wind turbines and farms on Doppler weather radars in Spain by increasing the dwell time to attain a higher temporal resolution of the data. Periodic signals were found in the Doppler returns depending on the alignment of the turbines with the radar beam. Using a similar technique for data collection, Isom *et al.* (2009) found that careful consideration needed to be made as turbine and precipitation spectra can occupy the same frequency span, so a technique was formed that utilised multiquadric interpolation in two and three dimensions. Hood *et al.* (2010) utilise fuzzy logic in addition to distinguishing features from Doppler radar data including spectral flatness and clutter phase alignment to identify the wind turbine locations, even during anomalous propagation. They also mention that the next step would be to analyse the effectiveness of polarimetric measurements for wind-farm identification.

In 2013 the UK Met Office began to upgrade the UK weather radar network to enable dual polarisation measurements which allow a greater capability of clutter identification. Gourley *et al.* (2007) use the textures of multiple polarimetric measurements followed by post-fuzzy reclassification based on the radial velocity, reflectivity and the differential phase shift to classify ground
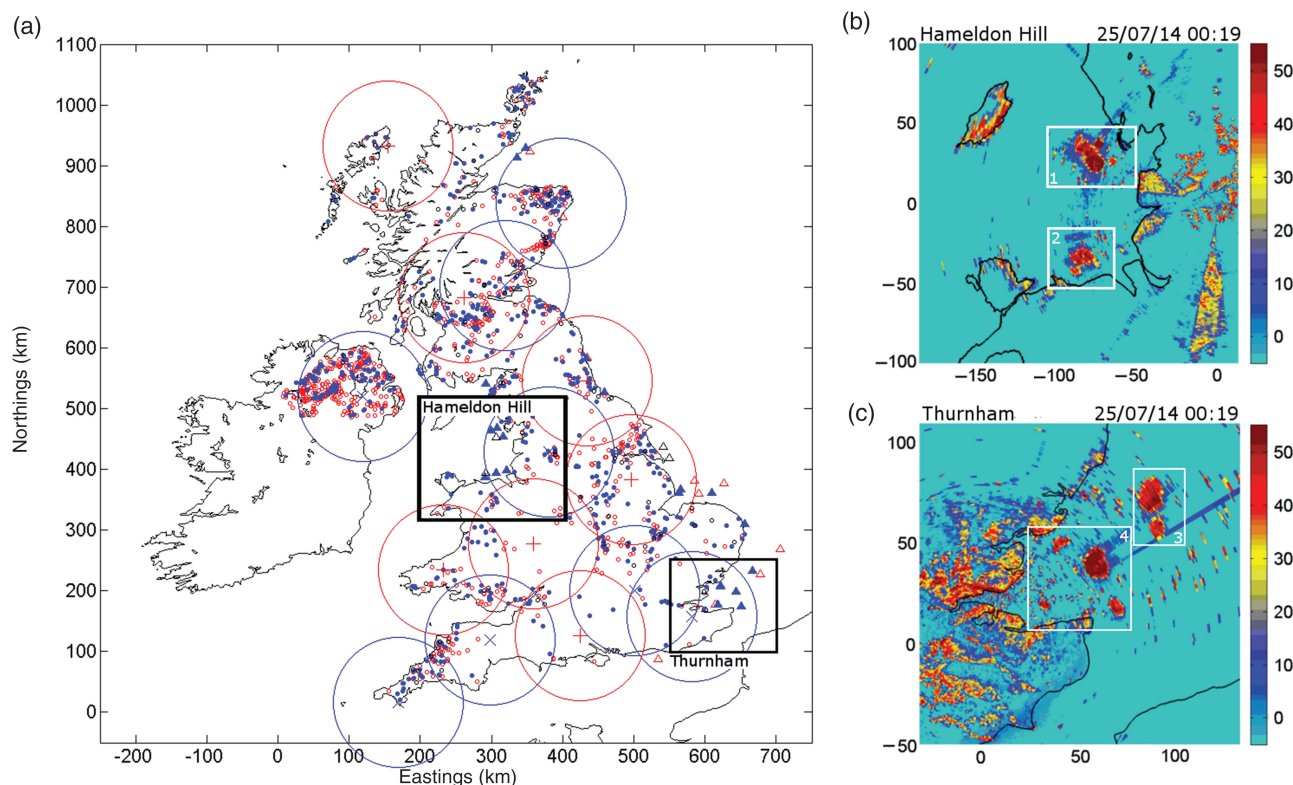
Figure 1. (a) Map of the United Kingdom including operational (filled) and planned and in construction (unfilled) onshore (dots) and offshore (triangles) wind farms. The circles show ranges of 100 km from the radars with dual polarized (X) and single polarized (+) with more upgraded from early 2016. (b) and (c) Zoomed-in sections of the respective Thurnham and Hameldon Hill radar scans at 0.5° elevations, with the white boxes encasing wind-farm clutter areas. Database of wind-farm and turbine locations from RenewableUK (2015).

clutter. They also make use of empirical class thresholds to suppress erroneous echo assignments. Fuzzy logic proves useful for ground-clutter identification (Berenguer *et al.*, 2006; Gourley *et al.*, 2007; Rico-Ramirez and Cluckie, 2008), and hydrometeor classification (Liu and Chandrasekar, 2000; Marzano *et al.*, 2007; Park *et al.*, 2009; Hall *et al.*, 2015). Hubbert *et al.* (2009) developed a fuzzy logic algorithm to remove standard propagation and anomalous propagation ground-clutter echoes using a novel clutter mitigation decision approach; however, they mention that this could not be applied to other clutter types, such as wind turbines. Some algorithms, such as Berenguer *et al.* (2006), apply a mask over the known areas of sea and land in order to use different algorithms for the two masks. This would create problems for offshore wind-farm clutter identification as the wind-farm clutter can vary in size and shape with different atmospheric and anomalous propagation conditions as shown later in this article.

The variance, or texture, of polarimetric variables has generally proven to be a useful metric for the classification of clutter (Giuli *et al.*, 1991; Ryzhkov and Zrnic, 1998; Chandrasekar *et al.*, 2013). Dufton and Collier (2015) use a fuzzy logic method with radial texture parameter inputs of dual polarisation variables including the correlation coefficient corrected for range effects and beam heights. Lakshmanan *et al.* (2014) use a 5 by 5 pixel area when computing textures, as in Park *et al.* (2009), as part of a neural network approach. In addition, inputs from radar moments at the given pixel, information from the vertical column, and outputs from a simple classifier are used. A further study, by Lakshmanan *et al.* (2015), investigates the contribution of each polarimetric variable to a method for discriminating between weather and non-weather echoes, finding the variance of differential reflectivity to overall perform slightly better than correlation coefficient due, in part, to the former having a greater resolution. Seo *et al.* (2015) similarly try to select variables by their ability to measure the underlying phenomena instead of relying solely on the statistical relationships inherent in fuzzy logic systems. They

avoid using radial velocity and spectrum width due to the non-zero Doppler signature from wind turbines as found in Mishra and Chandrasekar (2010). They instead focus on a smaller number of parameters and apply thresholds and supressed classes as in Gourley *et al.* (2007) and Lakshmanan *et al.* (2014).

Due to anomalous propagation of the radar beam during specific atmospheric conditions, some wind farms do not always affect the radar scans (Berenguer *et al.*, 2006); these cases have not been extensively examined (Seo *et al.*, 2015). As the wind-farm clutter regions vary, a static clutter map cannot be used; instead the echoes must be individually identified as clutter pixels. In this article, C-band dual polarimetric radar data will be used to propose a method for wind-farm identification and a current clutter classifier will be tested and compared to the updated version. A database of polarimetric measurements will be formed in order to observe the varied characteristics of the wind farms in comparison to other ground-clutter and precipitation echoes. The aim is to create a robust algorithm based on fuzzy logic to quickly classify the wind-farm clutter pixels in real time that can be applied easily to other operational weather radars within the UK network.

2. Data and statistical methods

Data from two operational C-band polarimetric weather radars have been analysed. These have been chosen due to their dual polarisation measurement capability and proximity to large offshore wind farms. The first is located at Hameldon Hill (Met Office, 2014) near Burnley, United Kingdom, and the second is positioned at Thurnham (Met Office, 2013), near London, United Kingdom. Hameldon Hill and Thurnham radars are part of the UK Met Office weather radar network, along with 16 other C-band radars (Met Office, 2009), of which ones in Jersey and Shannon, Ireland, are not shown in Figure 1. The scanning strategy for both radars includes five elevations of long-pulse (600 m) scans, of which only the lowest two have Linear Depolarisation Ratio (*LDR*) measurements, and six elevations of short-pulse

Table 1. Wind farm information proximate to the Hameldon Hill (groups 1 and 2) and Thurnham (groups 3 and 4) radars.

Box no.	Wind farm name	Range from nearest radar (km)	Area (km^2)	No of turbines	Power production (MW)	Total turbine height (m)
1.	Barrow	70	10	30	90	120
	Ormonde	85	10	30	150	163
	Walney P1 and P2	90	28	51	184	137
	West of Duddon Sands	80	67	108	389	150
2.	North Hoyle	85	10	30	60	107
	Rhyl Flats	90	10	25	90	134
	Gwynt y Mor	90	86	160	576	152
3.	Greater Gabbard	110	146	140	504	131
4.	Kentish Flats	35	10	30	90	115
	Gunfleet Sands	60	18	48	172	129
	Thanet	70	35	100	300	115
	London Array	67	100	175	630	147

The group numbers correspond to the boxes in Figure 1 (4C Offshore, 2016).

(300 m) scans. All elevations include measurements of horizontal reflectivity (Z_H), differential reflectivity (Z_{DR}), differential phase shift (Φ_{DP}), correlation coefficient (ρ_{HV}) and radial velocity (V_H). The lowest elevation scans of uncorrected reflectivity contain a large amount of ground-clutter contamination, as can be seen in Figure 1(c). The radars have a total range of 255 km with range bin lengths of 600 m and a beam width of 1°. These are shown as the labelled radars in Figure 1, in addition to the zoomed-in sections as part (b) and part (c) respectively. The wind-farm locations were cross-validated with a database of all constructed offshore and onshore wind farms (RenewableUK, 2015). It should be noted that the dots in Figure 1(a) can relate to small wind farms, or even single turbines, so the apparent high density in Northern Ireland would not be comparable to the offshore wind farms. The characteristics of the main wind-farm clusters that affect the two radars are shown in Table 1, and can be compared to the corresponding boxes in Figures 1(b) and (c).

As mentioned previously, a clutter map can help to reduce the continuously prevalent clutter regions; however, sometimes during anomalous propagation conditions a clutter tail or appears extending for up to 10 km behind the farm. This can be seen in Figure 1(c), behind the large wind farm in box 4. They are low reflectivity values of approximately 10 dBZ, but can reach up to 30 dBZ during severe anomalous propagation conditions. Norin (2015) finds a similar effect in Doppler radar measurements in Sweden. This increase in reflectivity behind the wind farm seems to be caused by multiple scattering effects, between the multiple turbines and between turbine and sea surface (Isom et al., 2009; Vogt et al., 2011; Norin, 2015). Multiple scattering is exacerbated by the rotating blades (Greving and Malkomes, 2006) and worsened further by the uneven sea surface. Another effect can be seen in Figure 1(b) within box 1 in which there appears to be a clutter tail but to the sides of the wind farms in an azimuthal direction. This seems to be caused by the side lobes of the beam hitting the wind farm as the half-power beam width section passes to either side.

Data were collected between March 2014 and April 2015, with half of the Thurnham dataset used for validation and half for initial calibration of the fuzzy logic algorithm described in the following sections. The Hameldon Hill data were then used as a second validation set. Long-term quality analysis of the UK Met Office radar network can be found in Harrison et al. (2014). Through examination of Φ_{DP} scans for multiple events there appears to be no data loss behind the wind farm due to blockage. This could be due to the wind farms only blocking a portion of the side lobes of the radar beam rather than the main section within the half-power beam width.

For each radar a ground-clutter probability map was formed to locate areas of ground clutter that occur most frequently in the radar scans. For Thurnham this is shown in Figure 2 with the off-shore wind farms located within the white boxes. This map shows how the frequency of occurrence during dry scans is much lower at 35−70% for the two farms located further from the radar. As the clutter tail and the more distant wind farm are variable, only a detection algorithm would work to detect and remove this clutter without unnecessarily removing precipitation through the use of a static map. Pixels that appeared over 80% of the time during clear-air days were used as the data collection points. The wind-farm dataset came from a mixture of permanent echoes and anomalous propagation echoes. Some of the wind farms only appear during anomalous propagation so a variety of times, seasons and atmospheric conditions were incorporated when testing the algorithm. A trained meteorologist separated precipitation pixels from clutter during different seasons and with a mixture of convective and stratiform rainfall events. Echoes that were clearly stationary between convective rainfall scans were identified as clutter and then sub-classified into wind-farm or ground clutter to then form the database of the separated wind-farm, ground-clutter and precipitation polarimetric measurements. The data collection was performed using software built specifically for this purpose.

In order to evaluate the ability of the algorithm to classify the echoes as precipitation or wind-farm clutter the Heidke Skill Score (HSS) will be used (EuMetCal, 2011). As explained in Schaefer (1990), the Critical Success Index (CSI) which is commonly used to indicate the value of warnings can be an overestimate of the forecast skill and not unbiased, so HSS will be used instead.

$$HSS = \frac{2 \cdot (a \cdot d - b \cdot c)}{(a + c) \cdot (c + d) + (a + b) \cdot (b + d)}, \quad (1)$$

where: a would be clutter correctly identified as clutter; b is precipitation incorrectly identified as clutter; c is clutter incorrectly identified as precipitation; and d is precipitation correctly determined to be precipitation.

3. Classifying wind-farm clutter

The collected datasets of wind-farm, precipitation and ground-clutter pixels were aggregated to form Probability Density Functions (PDF) for the Thurnham wind farms. Textures of Z_H, Z_{DR}, ρ_{HV} and Φ_{DP} were also calculated and collected for the same pixels. The texture values are obtained by taking the standard deviation of a 3×3 window area centred on the chosen pixel, which is an area that has been shown to work well in past research for a previous C-band radar installed at the same location (Rico-Ramirez and Cluckie, 2008). Clear-air pixels within the 3×3 area will be ignored when calculating the texture. In addition a Signal-to-Noise ratio threshold was used, with any noisy regions removed below a given threshold. Studies use different calculation areas due to different radar beam widths and range gates, though an approximate 1 km by 1 km window is considered appropriate, such as in Park et al. (2009) and Dufton and Collier (2015). High texture values imply a significant variability of polarimetric measurements within a small area which is usually associated with clutter regions as precipitation generally has a smoother appearance on radar scans (Rico-Ramirez and Cluckie, 2008).
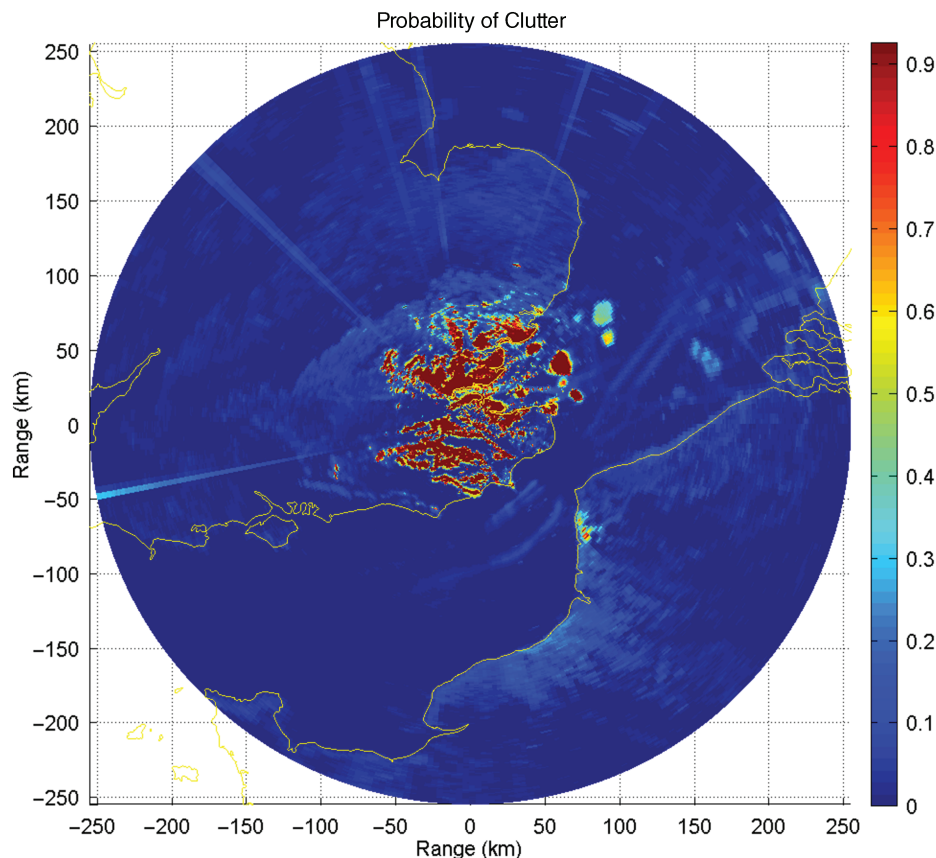
Probability of Clutter

Figure 2. Map showing the probability of reflectivity returns during dry clear-air days, where 0.9 would represent 9 in 10 scans having reflectivity returns for an individual pixel.

For echo classification the most useful variables will have the smallest overlap between the precipitation and clutter signals. The polarimetric variable ρ_{HV} and the textures of Φ_{DP}, ρ_{HV} and Z_{DR}, which are referred to as $t(\Phi_{DP})$, $t(\rho_{HV})$ and $t(Z_{DR})$ respectively, are generally agreed to have the greatest ability in identifying clutter echoes (Gourley *et al.*, 2007; Hubbert *et al.*, 2009; Islam *et al.*, 2012). However, as shown in Figure 3, these wind farms have a signal more similar to that of precipitation, especially for ρ_{HV}, $t(\rho_{HV})$, $t(\Phi_{DP})$ and *LDR*. The texture of the differential propagation phase $t(\Phi_{DP})$ here in the fuzzy logic algorithm has been used to help differentiate between clutter and precipitation, in a similar way to Bringi *et al.* (2011). They have used a standard deviation over a 10-gate moving window; however, this algorithm uses the texture over a 3 by 3 moving pixel window.

To form these empirical PDFs, approximately 200 000 ground-clutter pixels, 150 000 precipitation pixels and 100 000 wind-farm pixels were used. As noted by Lakshmanan *et al.* (2015) wind turbines can have values of ρ_{HV} close to unity, which is also a characteristic of precipitation, due to their thin vertical structure. This could cause problems with some older operational classification techniques that rely on standard ground-clutter PDFs for inputs.

Seo *et al.* (2015) use ρ_{HV} as a main initial classifier after separating out weaker reflectivity pixels (≤ 35 dBZ). This seems to work well for the onshore wind farms in the study but as shown in Figure 3 the empirical PDFs for ρ_{HV} are very similar for precipitation and these offshore wind farms so the application of that algorithm to these particular wind farms could be problematic. The textures of Z_{DR} and Φ_{DP} have a better discrepancy between wind farm and precipitation, but there is still more of an overlap than compared to normal ground clutter. *LDR*, Z_{DR} and ρ_{HV} have the most significant overlap of wind farm and precipitation distributions.

Interestingly for wind farms the V_H values here remain centred around zero with a small standard deviation, as shown in Figure 4, instead of having more variation and a non-zero signature, as in Norin (2015). To illustrate the differences in velocity, a block

of precipitation is found within box *a* of Figure 4, two wind farms in box *b*, and wind farms in box *c* surrounded by sea clutter displaying negative velocities of about 1.25 m s^{-1}. This is an unusual case with sea clutter in this region due to adverse anomalous propagation conditions, as modelling has shown the beam would not normally be hitting the water even at 0.3° (Rico-Ramirez *et al.*, 2009). These near-zero measurements could be due to having multiple wind turbines within each pixel, as beyond 50 km the pixels are broad enough to contain between 1 and 3 turbines. However the examples investigated by Norin (2015) also contain multiple turbines per pixel, yet they find an increase in the average absolute velocity once the turbines are built and operational. They suggest that the velocity frequency spectrum will be centred in a narrow peak around zero if multiple scattering between stationary parts of the turbine is dominant. Norin (2015) does find positive values of absolute radial velocity at the wind-farm sites; however, in that situation the beam directly hits the turbines at 0.5° and partially at 1.0°.

The individual wind farms surrounding the Thurnham radar can be seen to have different characteristics in the polarimetric measurements. Ten thousand data points were used per wind farm for the formation of these empirical PDFs in Figure 5. The textures of Φ_{DP}, Z_{DR} and V_H were all very similar between the different wind farms, but ρ_{HV}, *LDR*, and the textures of Z_H and ρ_{HV} all showed some significant variations. The differences between farms occur due to a combination of reasons. London Array (LA) wind turbines have heights of 147 m while Kentish Flats (KF) and Thanet (Th) are 115 m, in addition to different rotor diameters and tower thicknesses, which would affect the amount of backscatter from the side lobes and main radar beam. Another factor is the combination of distance of the farms from the radar, changing the coverage of one pixel from approximately 1 km^2 at 50 km to nearly 2 × 1 km^2 at 100 km. The turbine density within the wind farms also varies as Gunfleet Sands (GS), Kentish Flats and Thanet all have 3 turbines km^{-2}, whereas London Array has 1.5 turbines km^{-2}. The orientation of the blades and nacelle is altered with changing wind directions in order to maximise power
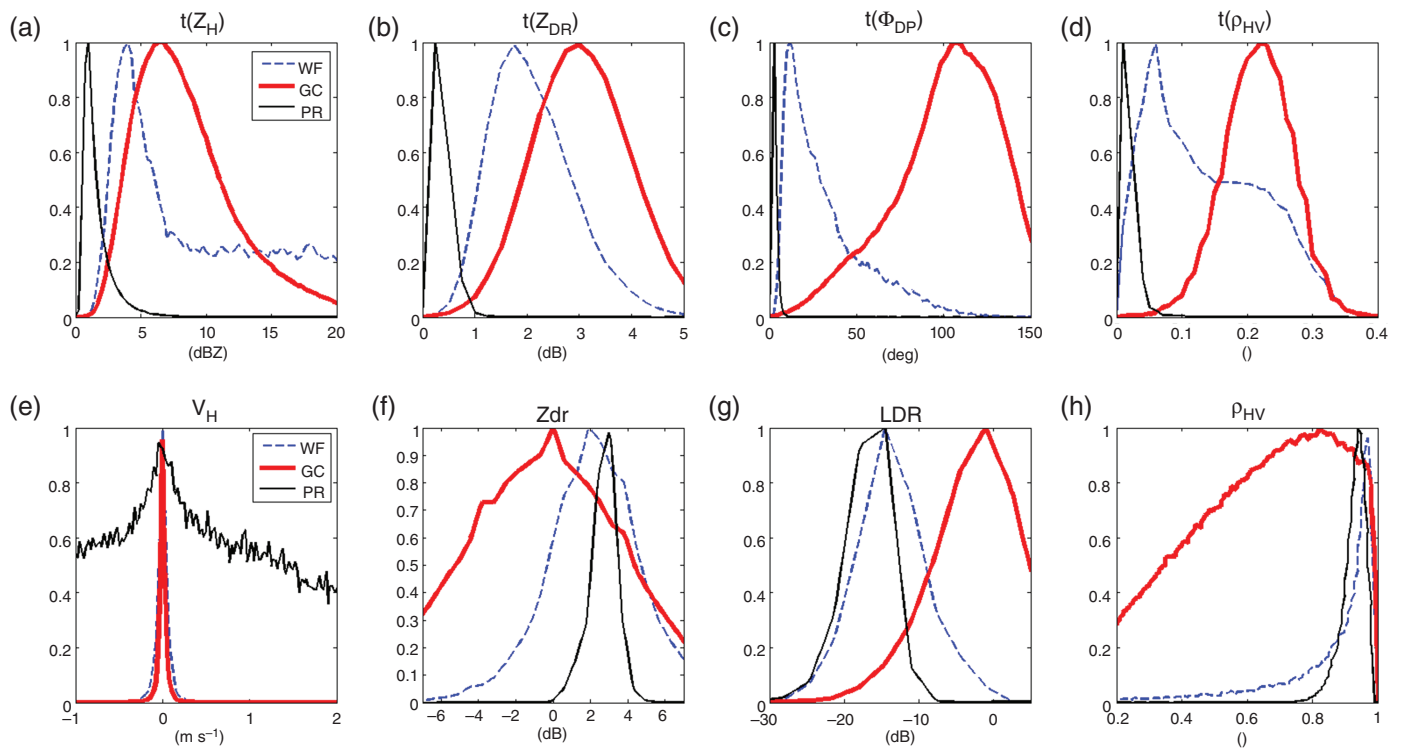
Figure 3. (a)–(h) Empirical Probability Density Functions (PDFs) of multiple variables for Wind Farms (WF), Ground Clutter and Anomalous Propagation echoes (GC), and Precipitation (PR) coloured in dashed blue, red, and black respectively. Here 't' represents the texture formed from the standard deviation of surrounding (3 × 3) pixels.
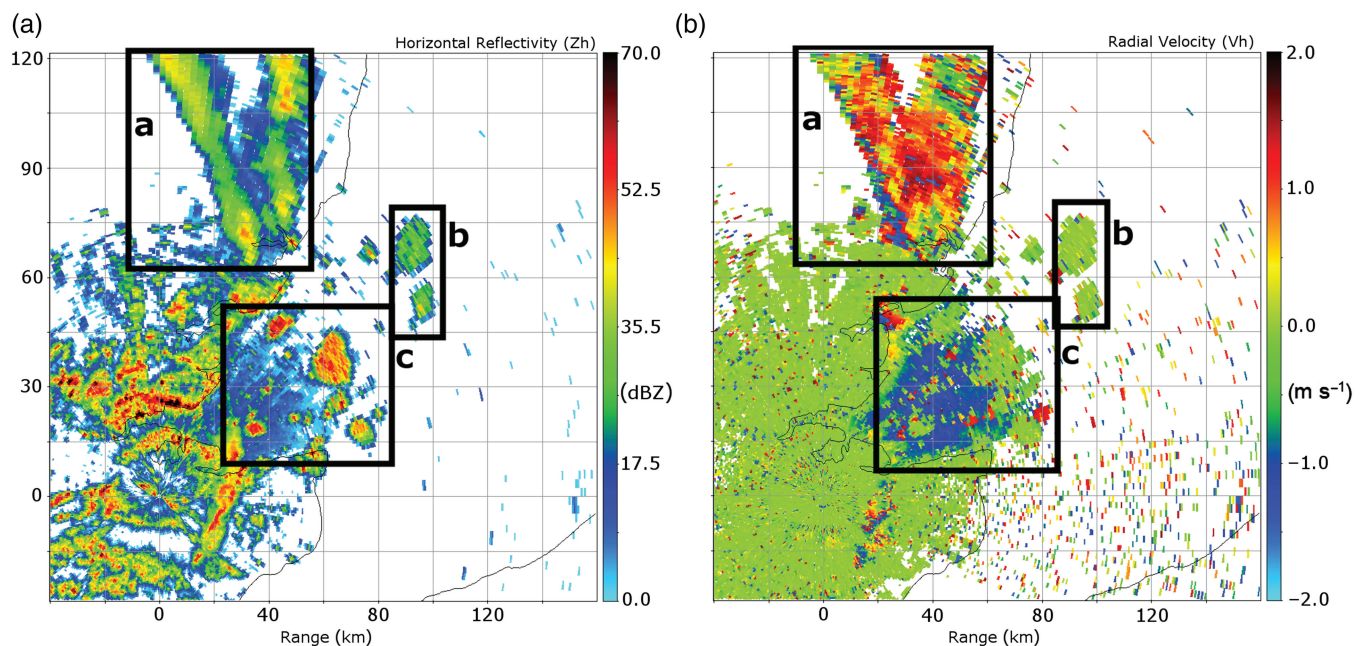

Figure 4. Uncorrected radar scans of (a) Horizontal Reflectivity and (b) Radial Velocity from 1449 UTC 10 August 2014. Box *a* shows convective precipitation with mixed velocities, box *b* shows the more distant wind farms, and box *c* contains wind farms amongst negative velocity sea clutter.

output (Schubel and Crossley, 2012). Mishra and Chandrasekar (2010) state the echo strength does vary with the alignment of radar beam with turbine rotation plane. The prevailing winds over the United Kingdom are from the southwest so the turbines will most frequently be oriented head on to the radar beam, creating the largest surface area of backscatter; however, there will still be variation between the wind farms. Due to difficulties obtaining the exact layouts of wind farms, and knowing the exact plane of observation of the turbine beyond the presumption of similarity with wind direction, it was not possible to analyse the effect of turbine plane of observation upon the echo characteristics. These changes in range, turbine density, turbine height, and orientation will affect the textures of polarimetric measurements.

This illustrates that multiple variables should be used in the final algorithm to identify the clutter echoes, as the use of a single or two variables could cause some incorrect classification.

Rico-Ramirez and Cluckie (2008) found that using normal ground-clutter membership functions to classify sea clutter yielded poor results, so the same is likely to be true for wind-farm echoes due to their differing PDFs in Figure 3. This could be fixed by using a mixture of wind-farm, sea-clutter and ground-clutter echoes to form an amalgamated PDF. These are shown in Figure 6, with the mixed ground clutter, sea clutter, and wind farm against precipitation values. Statistical results of using an amalgamation compared to a separation of the different clutter types will be shown in section 4.1. Empirical PDFs are used in
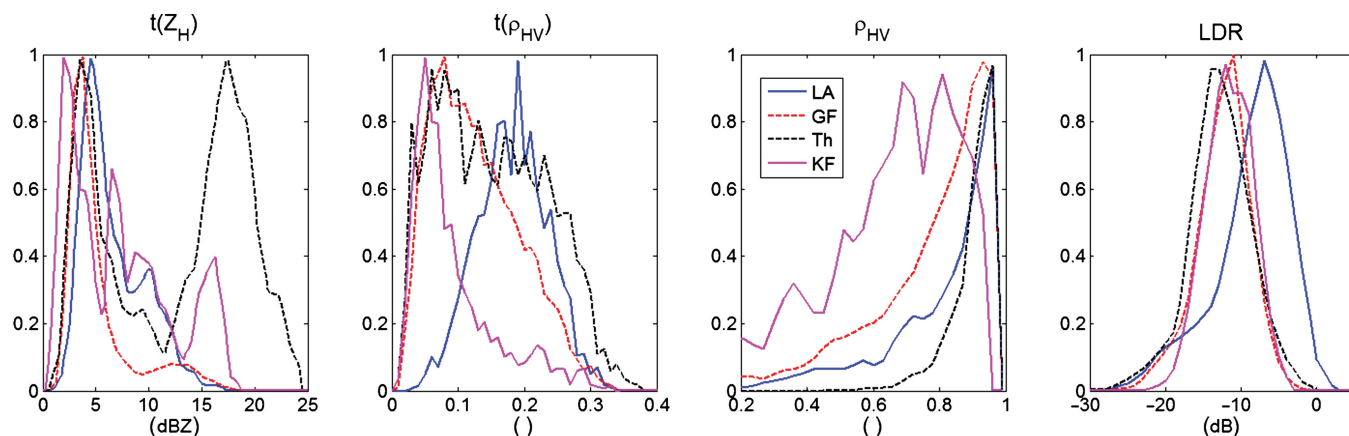
ⓒ 2016 The Authors. *Quarterly Journal of the Royal Meteorological Society*
published by John Wiley & Sons Ltd on behalf of the Royal Meteorological Society.

Q. J. R. Meteorol. Soc. (2016)

Figure 5. (a)–(d) Empirical Probability Density Functions (PDFs) of the four variables that contain varying values between the four main wind farms near Thurnham, called London Array (LA), Gunfleet Sands (GS), Thanet (Th) and Kentish Flats (KF).
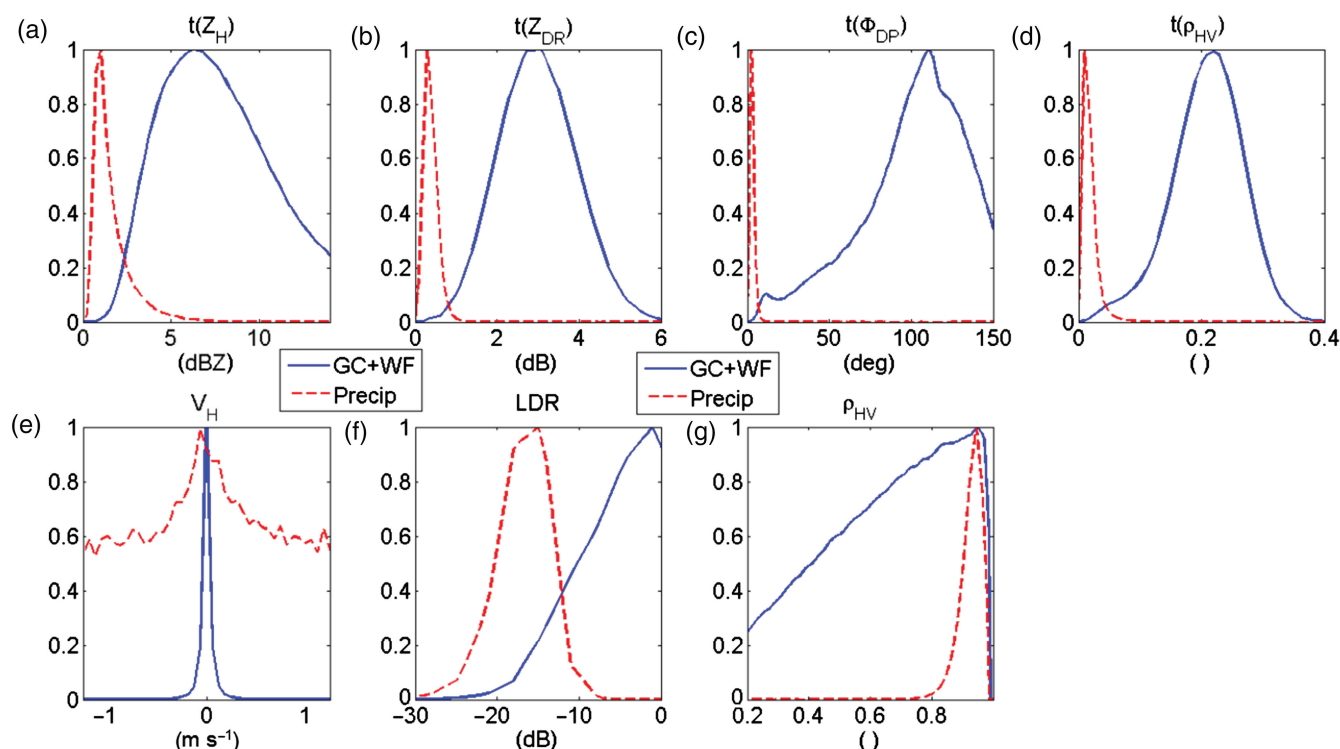

Figure 6. (a)–(g) Empirical Probability Density Functions (PDFs) of the seven variables used in the fuzzy logic algorithm.

the figures here just to help illustrate the differences between the signals. In the fuzzy logic algorithm these are converted into membership functions (MFs) in which all points are non-zero such that the product of all variables cannot be nullified. The fuzzy logic method is explained in detail by Mendel (1995).

Hameldon Hill radar is also affected by five onshore wind farms within a 10 km radius. The farms are much smaller than their offshore counterparts but still contain between 5 and 26 turbines each, which is enough to cause clutter echoes over nearly 100 pixels in close proximity to the radar. Data from these pixels were collected over the same period of dry days as the offshore wind farms with the resulting backscatter distributions shown in Figure 7. The backscatter distributions interestingly show a velocity signature centralised around zero with a very thin spread for the onshore wind farms in addition to high ρ_{HV} which is very different from previous research (Seo *et al.*, 2015), especially with small onshore farms. However it should be noted for comparison that Seo *et al.* (2015) use S-band WSR-88D radars. Gallardo-Hernando *et al.* (2008) use C-band Doppler weather radars and find non-zero signatures in the Doppler spectrum which they define as the power-weighted distribution of radial velocities within the resolution volume of the radar. The majority of research on wind turbine clutter analysis has

been focused on Doppler signatures (Gallardo-Hernando *et al.*, 2008; Hood *et al.*, 2010; Grande *et al.*, 2015) rather than C-band polarimetric signatures so a comparison is difficult. Thurnham is also affected slightly by onshore wind-farm clutter; however, it is more difficult to differentiate the farms from surrounding urbanised areas with other ground clutter due to the proximity to London.

3.1. Clutter in multiple elevations

There is some interference at higher elevations for the Thurnham radar, especially over the large central wind farm. This effect in Figure 8 could be due to anomalous propagation which can occur regularly, especially with the frequency of temperature inversions in summer mornings (Bodine *et al.*, 2011). It should be noted though that this is not an abnormal anomalous propagation case as it occurs regularly and can become much more severe. Norin (2015) finds a similar effect in Doppler radar measurements in Sweden. They analysed the beam height with distance to look for anomalous propagation and found that changes in height were only small in the area over the turbines. They suggest another possibility could be the radar beam scattering from increased levels of dust and turbulence above the turbine, but as seen in
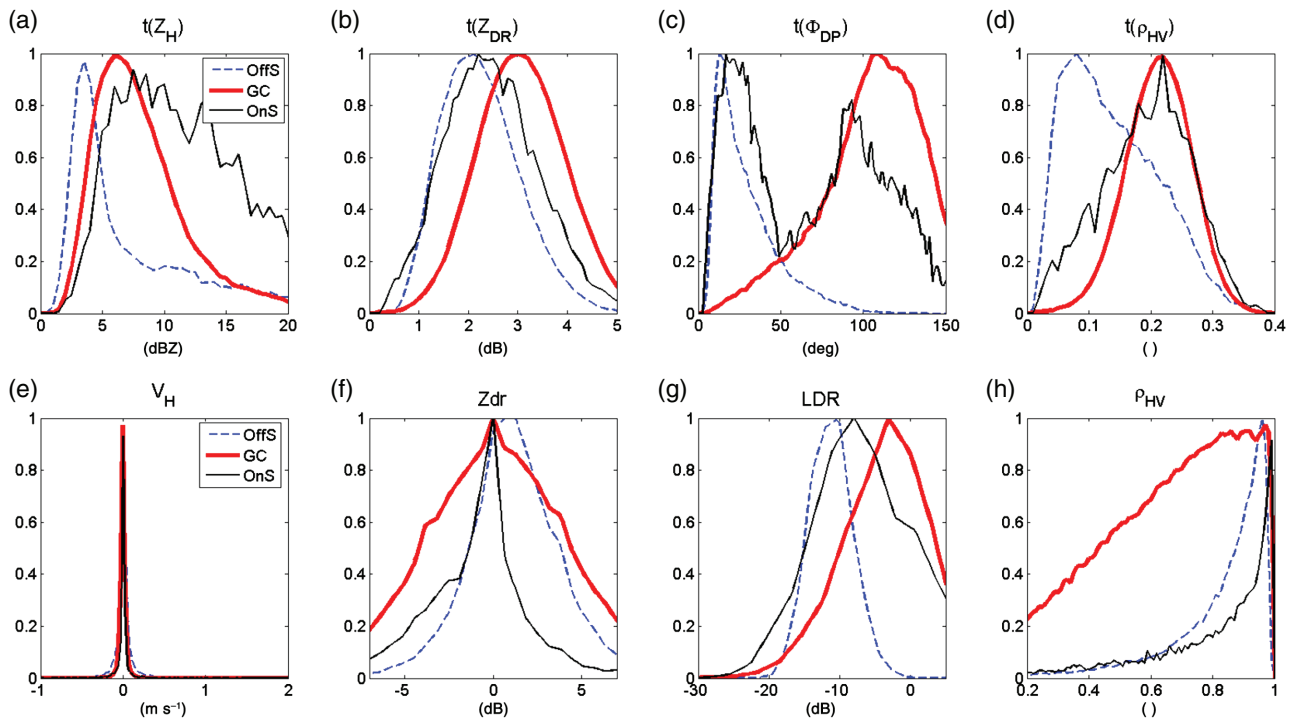
Figure 7. (a)–(h) Empirical Probability Density Functions (PDFs) for OffShore (OffS) and OnShore (OnS) wind farms in blue dashed and black respectively. Ground Clutter (GC) distributions are shown in red.
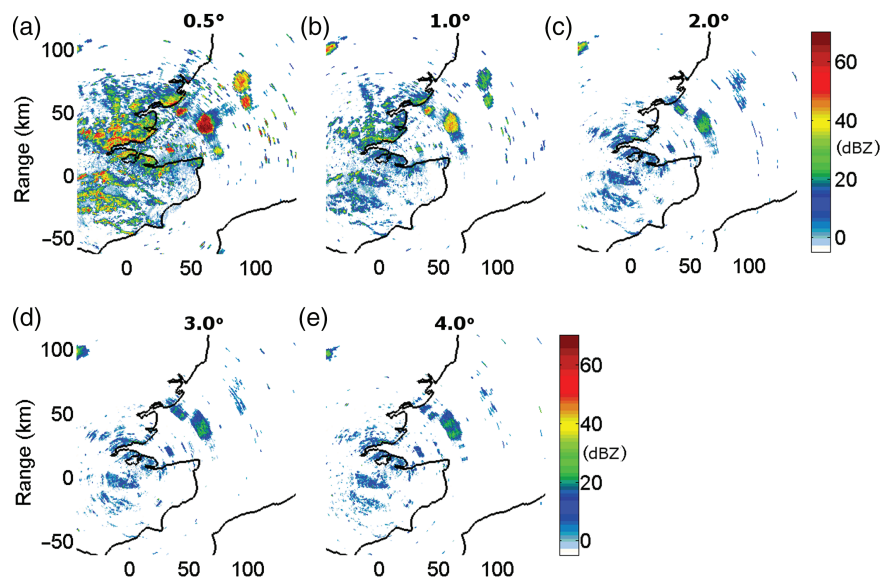

Figure 8. (a)–(e) Example of wind-farm clutter observed in reflectivity scans by the Thurnham radar at multiple elevations at 1320 UTC 23 June 2014.

Figure 8, the 4.0° elevation scan shows clutter even as the beam centre is approximately 5 km above the turbines. The most likely reason seems to be detection by the radar side lobes.

Wind turbines are known to create beam blockage effects in low-elevation scans (Norin and Haase, 2012) and considerably affect beam shape when positioned within 10 km of the radar (Belmonte and Fabregas, 2010). World Meteorological Organisation (WMO) guidelines state that beyond 45 km turbines are generally not observed, and that it is only an intermittent impact zone (WMO, 2010). The Operational Programme for the Exchange of weather RAdar information (OPERA) guidelines suggest 20 km as the furthest distance from C-band weather radars at which wind-farm projects need to be submitted for impact studies (OPERA, 2010). However as shown in Figure 8 there can be a notable impact on the radar scans even at a distance of 100 km. This is a complex problem as there is a continually growing need for renewable energy, and offshore wind farms can provide a large percentage of the total energy necessary for the United Kingdom (Sinden, 2007). Instead of restricting the building areas, perhaps

more should be researched into stealth techniques (Pinto *et al.*, 2010; Rashid and Brown, 2011), in addition to improved wind turbine identification algorithms. Reduction of side lobes would likely reduce the significance of turbine clutter effects.

During precipitation there is less of a problem, as seen in Figure 9, with significant clutter only affecting the lowest two elevations, and slight effects at 2.0°. This reinforces the need for an identification algorithm beyond a static clutter map as in this case higher-level precipitation would be unnecessarily removed. However, this causes an inability to replace precipitation at the lowest elevations with the elevations above, leaving holes in the data. Park and Berenguer (2015) account for the space–time variability of the precipitation field from clutter-corrected scans. The authors compare the value added by six different methods including interpolation and extrapolation in space and volumetric and temporal reconstruction. The usefulness of the different methods varies based on the precipitation types, for example with vertical extrapolation working well during deep convection due to smaller vertical gradients. A significant drawback for the
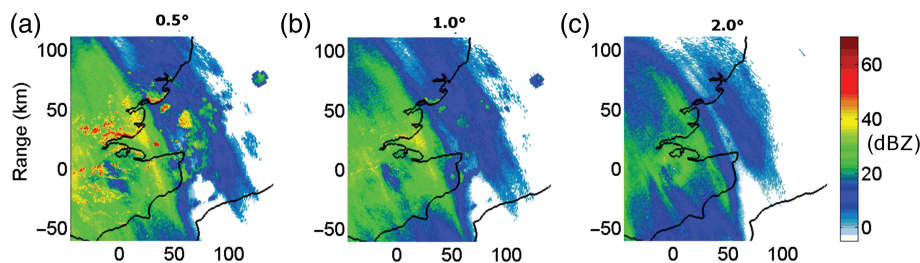
Figure 9. (a)–(c) Example of wind-farm clutter observed during precipitation in reflectivity scans by the Thurnham radar at multiple elevations at 1740 UTC 26 December 2014.
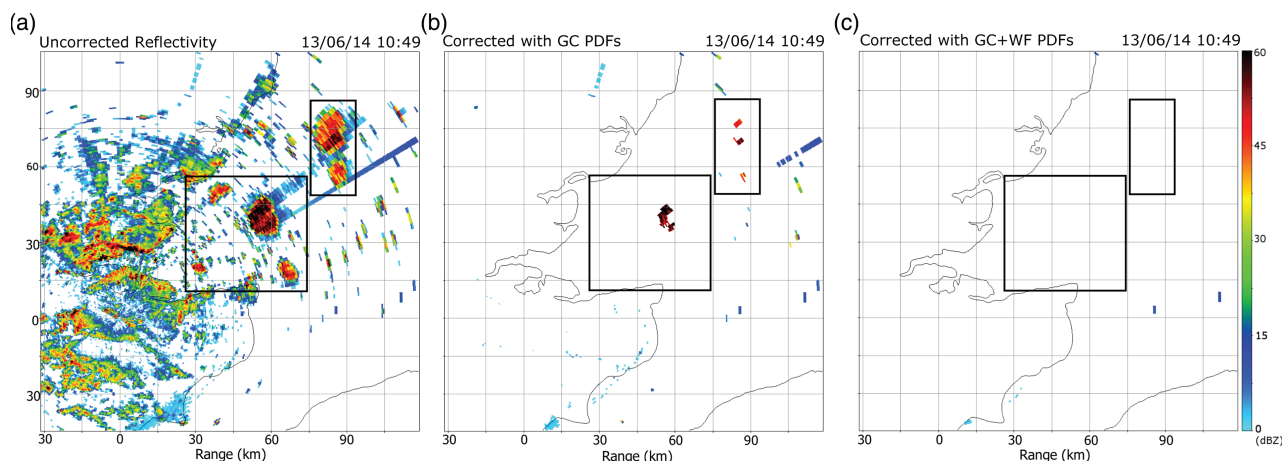

Figure 10. (a) Uncorrected clutter-only Thurnham radar scan showing clutter echoes, including two large wind-farm clusters. (b) Scans corrected with the original ground-clutter PDFs, and (c) the new PDFs that include wind-farm measurements.

application of this method for the large wind farms in this case would be due to the size and shape of the clutter, as there is a single block of around 150 pixels which would make interpolation very difficult, in particular during convective precipitation.

4. Clutter removal

4.1. Thurnham validation

A method described in Rico-Ramirez and Cluckie (2008), based on PDFs obtained from an earlier version of the Thurnham radar, was initially used to try to identify the wind-farm clutter and used as a benchmark on which to compare the new classifier. This algorithm uses fuzzy logic and all available polarimetric variables and textures to determine the echo types at each pixel. However due to the usage of PDFs that consisted of data collected only from standard ground clutter, the algorithm failed to remove the entirety of the wind farms, shown in Figure 10. The wind farms have a smoother appearance and lower texture values so the algorithm classified them as precipitation rather than clutter. With the addition of the wind-farm clutter dataset to form an amalgamated ground-clutter and wind-farm PDF the same algorithm then fully identified and removed the wind-farm regions (Figure 10(c)).

The ability of the algorithm to keep true precipitation pixels needs to be tested. There are no available rain-gauges off the coast in the wind-farm regions, so the truth comes from the validation sets of precipitation, ground-clutter and wind-farm measurements from Thurnham. A total of 160 000 precipitation and wind-farm clutter pixels from events of differing synoptic conditions and seasons were used as validation. Different combinations of the seven empirical PDF variables (Figure 6) will be used to observe which variable set is most proficient for wind-farm identification.

Using the new empirical PDFs, which include the collected wind-farm data, there is a noticeable improvement in HSS for all of the variable combinations shown in Table 2. Due to the similarity between the precipitation and wind-farm

Table 2. HSS and FAR statistics for the classifiers combining different inputs for the Thurnham validation data set.

Using either GC or both GC and WF data	GC		GC and WF	
	HSS (%)	False PR (%)	HSS (%)	False PR (%)
1. All	67.4	0.05	96.8	1.24
2. $t(Z_{DR})$, $t(\Phi_{DP})$ and V_H	57.9	0.05	93.1	0.46
3. $t(Z_H)$, $t(\rho_{HV})$ and V_H	88.6	9.70	90.9	1.08
4. $t(Z_H)$, $t(Z_{DR})$, $t(\rho_{HV})$, $t(\Phi_{DP})$ and V_H	43.1	0.05	95.8	1.16

Here 't' represents the texture of that variable. Methods using only Ground Clutter (GC) in PDFs are compared to using both GC and Wind Farm (WF) data in PDFs.

signals a new metric is added which shows the percentage of precipitation (PR) pixels incorrectly classified as clutter (FalsePR). The FalsePR values here however are similar to those obtained by Seo *et al.* (2015) through the use of a decision tree approach using carefully considered variables. They find a large increase in the misidentification of precipitation pixels beyond 100 km due in part to beam broadening and overshooting at that range.

The usage of all variables results in a slightly lower HSS; however as mentioned in Rico-Ramirez and Cluckie (2008) it can be more robust to use all variables instead of relying only on a small number of polarimetric measurements due to possible complications with some radar measurements, such as noise. As the Wind Farm (WF) and Ground Clutter (GC) signals are very different for $t(\Phi_{DP})$ and slightly for $t(\rho_{HV})$ there is a substantial change in HSS in combination 4 when the WF data are included in the classification.

Sea clutter can be identified due to its properties of low ρ_{HV} (<0.6) and a high frequency of non-zero radial velocity signatures (Rico-Ramirez and Cluckie, 2008). This can cause a problem with the usage of these empirical PDFs as non-zero velocity values are associated strongly with rainfall. In addition both sea clutter and rainfall have low reflectivity textures, so the decision was made

to not amalgamate sea clutter with ground and wind-farm clutter as there would be too much overlap with precipitation. The results of a test to compare the amalgamation of clutters against separated membership functions are shown in Table 3. For this case only 10 000 sea-clutter validation pixels could be used, as sea clutter is a rare occurrence causing small numbers of relatively low reflectivity pixels, so for this test 10 000 of each clutter type were compared with 30 000 precipitation pixels. When all variables are used the HSS and FalsePR values are similar; however, problems arise for the sea-clutter (SC) separation method as fewer variables are used with a steep increase in FalsePR percentages. The texture of Φ_{DP} proves to be valuable while $t(Z_H)$ and $t(\rho_{HV})$ show lesser value with minimal change in classifier ability between combinations 4 and 2. The ability for the algorithm to be robust even with fewer variables is important as LDR is not available for every scan, and sometimes operational difficulties occur when measuring some variables (Rico-Ramirez and Cluckie, 2008).

Figure 11 shows three examples of classification outputs from corresponding reflectivity scans. For this classification all variables are used in addition to a clutter probability map which is shown as Figure 2. The probabilities from the map will be used as a multiplier within the fuzzy logic algorithm. This map was formed from 50 days of clear-air scans spread over the course of a year. Figures 11(a) and (d) show some problems with identification of pixels in the edges of the central convective band being classified incorrectly as clutter, but all but one are low reflectivity values on the edges of the noisy band. This illustrates the downsides of the WF and GC merging as it seems to fare more poorly with noisy areas or highly textured convective regions; however, it still correctly classifies a vast majority of the precipitation pixels, especially those in the central higher reflectivity areas. The classification scheme seems to work well for the stratiform cases in parts (b) and (c), with the noisier edge regions of the precipitation bands being classified as rainfall.

Table 3. HSS and FAR statistics for the classifiers combining different inputs for the Thurnham validation dataset.

Variable combinations	SC separated		SC amalgamated	
	HSS (%)	False PR (%)	HSS (%)	False PR (%)
1. All	97.5	1.4	97.1	1.1
2. $t(Z_{DR})$, $t(\Phi_{DP})$ and V_H	80.7	12.4	85.3	0.5
3. $t(Z_H)$, $t(\rho_{HV})$ and V_H	63.8	34.7	75.2	1.5
4. $t(Z_H)$, $t(Z_{DR})$, $t(\rho_{HV})$, $t(\Phi_{DP})$ and V_H	85.8	12.4	87.1	1.2
5. $t(Z_H)$, $t(Z_{DR})$, $t(\rho_{HV})$, $t(\Phi_{DP})$	78.2	27.4	93.7	3.2

Here 't' represents the texture of that variable. Methods using an amalgamation of Sea Clutter (SC), Ground Clutter (GC) and Wind Farm clutter (WF) in PDFs are compared to using GC and WF amalgamated with SC separate in PDFs.

4.2. Hameldon Hill validation

To test the ability of the algorithm it has also been applied to a different radar within the UK Met Office network. The two radars have similar characteristics; however, the more recently upgraded Hameldon Hill radar has an updated antenna. The Thurnham radar produced a peak ρ_{HV} of 0.9775 in rain, whereas the Hameldon Hill radar reached a higher peak of 0.9985 while having a smaller Z_{DR} offset and higher-quality LDR measurements (Adams *et al.*, 2015). The PDFs are unchanged from the Thurnham radar. Figure 12 shows that there is again a significant improvement in clutter removal when the wind-farm measurements are added to the PDFs with all wind-farm and ground clutter being removed.

The statistics associated with the different classifier combinations are shown in Table 4. Again, there is an increase in false classification of precipitation pixels (FalsePR), and an increase in HSS for all combinations when the wind-farm measurements are added. Using all variables (combination 1) and also combination 4 are notably very good for HSS and FalsePR, with combination 1
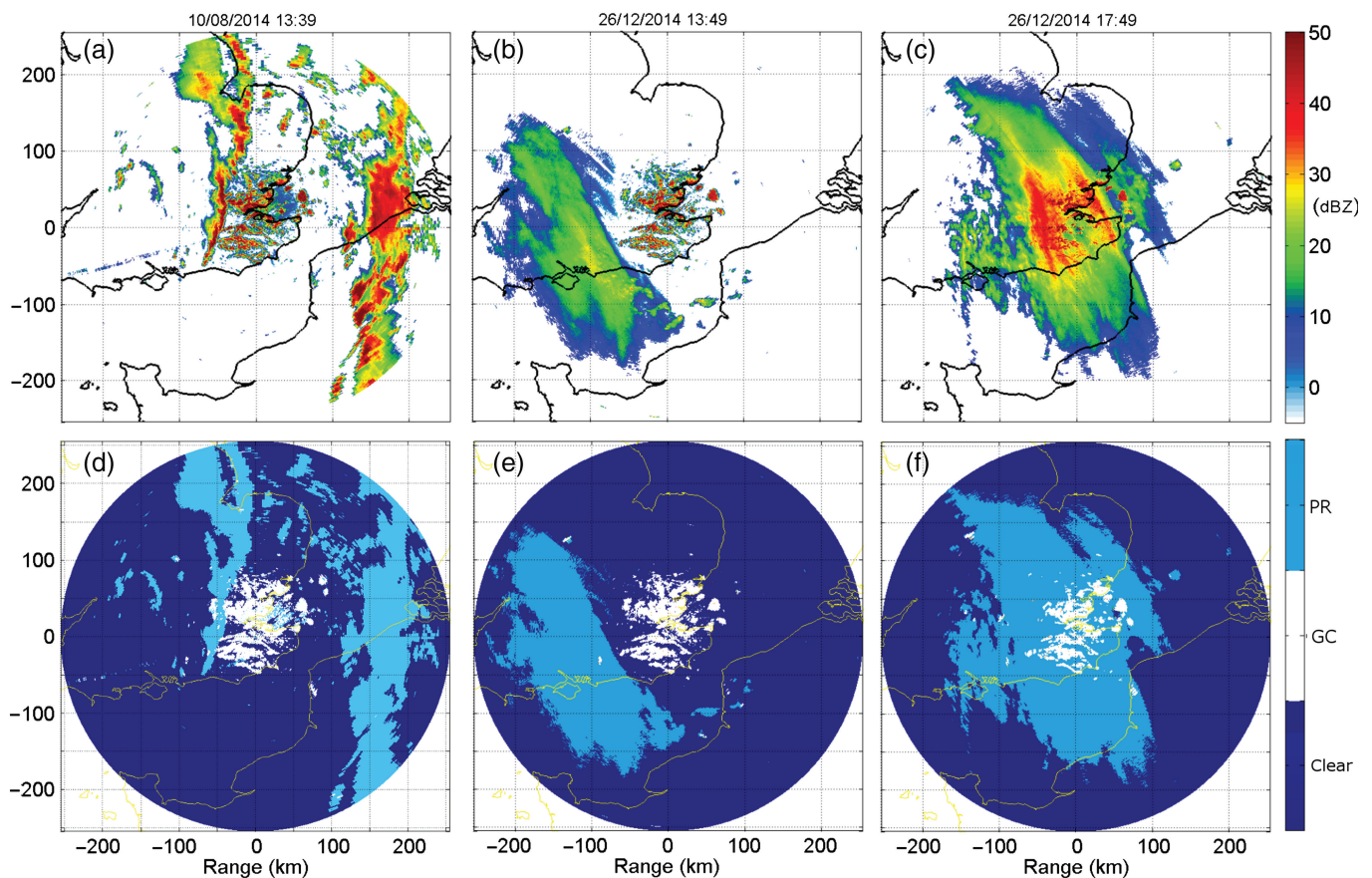

Figure 11. (a)–(c) Uncorrected radar scans displaying bands of precipitation during three events approaching the Thurnham radar with (d)–(f) echo classification outputs.
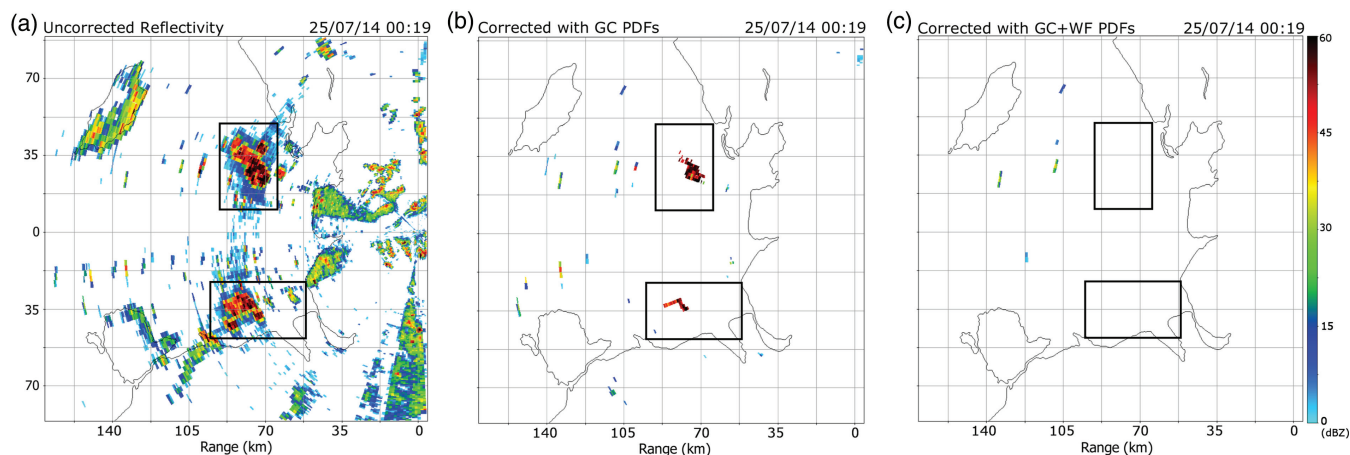
ⓒ 2016 The Authors. *Quarterly Journal of the Royal Meteorological Society* published by John Wiley & Sons Ltd on behalf of the Royal Meteorological Society.

Q. J. R. Meteorol. Soc. (2016)

Figure 12. (a) Uncorrected clutter-only Hameldon Hill radar scan showing clutter echoes, including two large wind-farm clusters. (b) Scans corrected with the original ground-clutter PDFs, and (c) the new PDFs that include wind-farm measurements.

Table 4. HSS and FAR statistics for the classifiers combining different inputs for the Hameldon Hill validation dataset.

Using either GC or both GC and WF data	GC		GC and WF	
	HSS (%)	False PR (%)	HSS (%)	False PR (%)
1. All	58.4	0.02	96.9	0.69
2. $t(Z_{DR})$, $t(\Phi_{DP})$ and V_H	49.7	0.07	85.8	0.78
3. $t(Z_H)$, $t(\rho_{HV})$ and V_H	80.2	9.84	92.7	1.40
4. $t(Z_H)$, $t(Z_{DR})$, $t(\rho_{HV})$, $t(\Phi_{DP})$ and V_H	42.4	0.09	92.3	0.10

Here 't' represents the texture of that variable. Methods using only Ground Clutter (GC) in PDFs are compared to using both GC and Wind Farm (WF) data in PDFs.

performing the best overall. Perhaps unexpectedly the classification statistics are better for Hameldon Hill than Thurnham, even though the PDF data were taken from the Thurnham dataset. Using all variables the HSS is similar between Hameldon Hill and Thurnham; however, the FalsePR value shows some bigger differences. The algorithm struggles more with the correct identification of precipitation for the Thurnham radar which is perhaps due to the poorer antenna quality (as shown by the maximum ρ_{HV} value in rain) leading to noisier edges of the precipitation areas. In all combinations the Hameldon Hill validation set has noticeably fewer incorrectly classified precipitation pixels with the low FalsePR values. This demonstrates a very good and promising ability for using the algorithm and PDFs for other radars in the network.

5. Conclusion

Essentially, the findings are that the wind-farm PDFs are different to the normal ground-clutter distributions with some significant overlap with precipitation distributions for some variables, and thus this needs to be accounted for when removing clutter. For most wind-farm cases it is suitable to use a basic clutter probability map which would greatly aid in the wind-farm removal but due to the presence of large wind farms that only appear during anomalous propagation, the clutter maps cannot be entirely relied upon. The operational weather radars need to be able to quickly and easily classify the anomalous propagation wind farms and correctly leave the true precipitation pixels. Ideally the same algorithm and method should be applicable to all connected weather radars in the network without having to change any limits that can cause incorrect classification due to the need for separate calibration for each radar. Thus a fuzzy logic approach works well due to the robust nature of the algorithm. New farms are built, which will continually be the case as many new and larger wind farms are proposed each year to account for the

continually increasing renewable energy demands. These different wind farms can have very different backscatter properties based on their distance from the radar and the density of the wind turbines. So an approach based on these limits could cause future problems. Further, due to the problem of multiple scattering effects, a variable clutter tail that results in reflectivity values of up to 30 dBZ nullifies the use of a static clutter map. The usage of this robust algorithm that can detect the wind-farm clutter in real time through the use of multiple polarimetric measurements would be beneficial.

World Meteorological Organisation guidelines on weather radar and turbine sites state that at 20−45 km the turbines are generally visible in lowest scan with low impact, and beyond 45 km they are generally not observed but can be due to propagation conditions. This is likely the case for single turbines or small onshore wind farms; however, larger farms should possibly have their own guidelines for placement as they are continually visible even at ranges of up to 90 km.

The method is able to be transferred to other radars within the network without recalibration of the membership functions, as shown by the high HSS values in the Hameldon Hill validation set. New wind farms, larger than the London Array, are planned and in construction in the Moray Firth and near the Norfolk Coast, which would affect other polarimetric radars in the following years. These larger farms could have even more significant multiple scattering effects leading to larger holes in radar data over the North Sea. However, this algorithm only identifies clutter areas in weather radar measurements, but additional work has to be done on how to interpolate these clutter areas with adequate rainfall measurements.

References

4C Offshore. 2016. 'Off shore energy consultancy'. http://www.renewableuk.com/en/renewable-energy/wind-energy/uk-wind-energy-database (accessed 1 July 2014).

Adams D, Darlington T, Sugier J, Kitchen M, Sloan C. 2015. 'Importance of antenna characteristics to radar performance.' Paper 265 In *Proceedings of the 37th Conference on Radar Meteorology*, 14−18 September 2015, Norman, OK. American Meteorological Society: Boston, MA.

Angulo Pita I, Grande O, Jenn D, Guerra Pereda D, De la Vega Moreno D. 2015. Estimating reflectivity values from wind turbines for analyzing the potential impact on weather radar services. *Atmos. Meas. Tech.* **8**: 2183−2193, doi: 10.5194/amt-8-2183-2015.

Belmonte A, Fabregas X. 2010. Analysis of wind turbines blockage on Doppler weather radar beams. *IEEE Antennas Wirel. Propag. Lett.* **9**: 670–673, doi: 10.1175/LAWP.2010.2057238.

Berenguer M, Sempere-Torres D, Corral C, Sánchez-Diezma R. 2006. A fuzzy logic technique for identifying nonprecipitating echoes in radar scans. *J. Atmos. Oceanic Technol.* **23**: 1157–1180, doi: 10.1175/JTECH1914.1.

Bodine D, Michaud D, Palmer RD, Heinselman PL, Brotzge J, Gasperoni N, Cheong BL, Xue M, Gao J. 2011. Understanding radar refractivity: Sources of uncertainty. *J. Appl. Meteorol. Climatol.* **50**: 2543–2560, doi: 10.1175/2011JAMC2648.1.

Bringi VN, Rico-Ramirez MA, Thurai M. 2011. Rainfall estimation with an operational polarimetric C-band radar in the United Kingdom: comparison with a gauge network and error analysis. *J. Hydrometeorol.* **12**: 935–954, doi: 10.1175/JHM-D-10-05013.1.

Chandrasekar V, Keränen R, Lim S, Moisseev D. 2013. Recent advances in classification of observations from dual polarization weather radars. *Atmos. Res.* **119**: 97–111, doi: 10.1016/j.atmosres.2011.08.014.

Dufton DRL, Collier CG. 2015. Fuzzy logic filtering of radar reflectivity to remove non-meteorological echoes using dual polarization radar moments. *Atmos. Meas. Tech. Discuss.* **8**: 5025–5063, doi: 10.5194/amt-8-3985-2015.

EuMetCal. 2011. 'Heidke Skill Score (HSS) forecast verification'. http://www.eumetcal.org/resources/ukmeteocal/verification/www/english/msg/ver_categ_forec/uos3/uos3_ko1.htm (accessed 14 July 2016).

Gallardo-Hernando B, Perez-Martinez F, Aguado-Encabo F. 2008. 'Statistical characterization of wind turbine clutter in C-band radars.' In *Proceedings of the 2008 International Conference on Radar*, 2–5 September 2008. IEEE: Adelaide, Australia, pp. 360–364.

Gallardo-Hernando B, Muñoz-Ferreras J-M, Perez-Martinez F, Aguado-Encabo F. 2011. Wind turbine clutter observations and theoretical validation for meteorological radar applications. *IET Radar Sonar Navig.* **5**: 111–117, doi: 10.1049/iet-rsn.2009.0296.

Giuli D, Gherardelli M, Freni A, Seliga TA, Aydin K. 1991. Rainfall and clutter discrimination by means of dual-linear polarization radar measurements. *J. Atmos. Oceanic Technol.* **8**: 777–789, doi: 10.1175/1520-0426(1991)008<0777:RACDBM>2.0.CO;2.

Gourley JJ, Tabary P, Parent du Chatelet J. 2007. A fuzzy logic algorithm for the separation of precipitating from nonprecipitating echoes using polarimetric radar observations. *J. Atmos. Oceanic Technol.* **24**: 1439–1451, doi: 10.1175/JTECH2035.1.

Grande O, Angulo I, Jenn D, Aguado F, Guerra D, de la Vega D. 2015. 'Analysis of wind turbines radar cross section for analyzing the potential impact on weather radars'. In *2015 9th European Conference on Antennas and Propagation (EuCAP)*. Lisbon, Portugal, pp. 1–5.

Greving G, Malkomes M. 2006. 'On the concept of the radar cross section RCS of distorting objects like wind turbines for the weather radar'. In *Proceedings Fourth European Conference on Radar in Meteorology and Hydrology*. European Meteorological Society: Barcelona, Spain, P5.8.

Hall W, Rico-Ramirez MA, Kramer S. 2015. Classification and correction of the bright band using an operational C-band polarimetric radar. *J. Hydrol.* **531**: 248–258, doi: 10.1016/j.jhydrol.2015.06.011.

Harrison D. 2012. 'Impact of operational wind farms in the United Kingdom on weather radar products'. In Proceedings of the 7th European Conference on Radar in Meteorology and Hydrology (ERAD 2012), 24–29 June 2012. Toulouse, France.

Harrison D, Georgiou S, Gaussiat N, Curtis A. 2014. Long-term diagnostics of precipitation estimates and the development of radar hardware monitoring within a radar product data quality management system. *Hydrol. Sci. J.* **59**: 1327–1342, doi: 10.1080/02626667.2013.841316.

Hood K, Torres S, Palmer R. 2010. Automatic detection of wind turbine clutter for weather radars. *J. Atmos. Oceanic Technol.* **27**: 1868–1880, doi: 10.1175/2010JTECHA1437.1.

Hubbert JC, Dixon M, Ellis SM. 2009. Weather radar ground clutter. Part II: Real-time identification and filtering. *J. Atmos. Oceanic Technol.* **26**: 1181–1197, doi: 10.1175/2009JTECHA1160.1.

Islam T, Rico-Ramirez MA, Han D, Srivastava PK. 2012. Artificial intelligence techniques for clutter identification with polarimetric radar signatures. *Atmos. Res.* **109**: 95–113, doi: 10.1016/j.atmosres.2012.02.007.

Isom BM, Palmer RD, Secrest GS, Rhoton RD, Saxion D, Alimon TL, Reed J, Crum R, Vogt R. 2009. Detailed observations of wind turbine clutter with scanning weather radars. *J. Atmos. Oceanic Technol.* **26**: 894–910, doi: 10.1175/2008JTECHA1136.1.

Lakshmanan V, Karstens C, Krause J, Tang L. 2014. Quality control of weather radar data using polarimetric variables. *J. Atmos. Oceanic Technol.* **31**: 1234–1249, doi: 10.1175/JTECH-D-13-00073.1.

Lakshmanan V, Karstens C, Krause J, Elmore K, Ryzhkov A. 2015. Which polarimetric variables are important for weather/no-weather discrimination? *J. Atmos. Oceanic Technol.* **32**: 1209–1223, doi: 10.1175/JTECH-D-13-00205.1.

Liu H, Chandrasekar V. 2000. Classification of hydrometeors based on polarimetric radar measurements: development of fuzzy logic and neuro-fuzzy systems, and *in situ* verification. *J. Atmos. Oceanic Technol.* **17**: 140–164, doi: 10.1175/1520-0426(2000)017<0140:COHBOP>2.0.CO;2.

Marzano FS, Scaranari D, Vulpiani G. 2007. Supervised fuzzy-logic classification of hydrometeors using C-band dual-polarized radars. *IEEE Trans. Geosci. Remote Sensing* **45**: 3784–3799, doi: 10.1109/TGRS.2007.903399.

Mendel JM. 1995. Fuzzy logic systems for engineering: a tutorial. *Proc. IEEE* **83**: 345–377, doi: 10.1109/5.364485.

Met Office. 2009. 'Weather radar fact sheet number 15'. http://www.metoffice.gov.uk/media/pdf/j/h/Fact_sheet_No._15.pdf (accessed 14 July 2016).

Met Office. 2013. 'Thurnham C-band rain radar dual polar products'. NCAS British Atmospheric Data Centre, 2015. http://catalogue.ceda.ac.uk/uuid/c2d682651d6b4fcf98466eb71cd02ef1 (accessed 20 March 2015).

Met Office. 2014. 'Hameldon Hill C-band rain radar dual polar products'. NCAS British Atmospheric Data Centre, 2015. http://catalogue.ceda.ac.uk/uuid/d8a66e1e1b50495c9d3066b7c5919688 (accessed 20 March 2015).

Mishra KV, Chandrasekar V. 2010. 'Signal analysis and modelling of wind turbine clutter in weather radars'. In *2010 IEEE International Geoscience and Remote Sensing Symposium (IGARSS)*. IEEE, 3561–3564, doi: 10.1109/IGARSS.2010.5652123.

Norin L. 2015. A quantitative analysis of the impact of wind turbines on operational Doppler weather radar data. *Atmos. Meas. Tech.* **8**: 593–609, doi: 10.5194/amt-8-593-2015.

Norin L, Haase G. 2012. Doppler weather radars and wind turbines. In *Doppler Radar Observations*, Bech J. (ed.): 333–354. InTech Open Access Publisher: Rijeka, Croatia and Shanghai, China.

OPERA. 2010. 'Statement of the OPERA group on the cohabitation between weather radars and wind turbines'. http://www.eumetnet.eu/sites/default/files/OPERA_2010_14_Statement_on_weather_radars_and_wind_turbines.pdf (accessed 1 February 2016).

Park S, Berenguer M. 2015. Adaptive reconstruction of radar reflectivity in clutter-contaminated areas by accounting for the space–time variability. *J. Hydrol.* **520**: 407–419, doi: 10.1016/j.jhydrol.2014.11.013.

Park HS, Ryzhkov AV, Zrnic DS, Kim KE. 2009. The hydrometeor classification algorithm for the polarimetric WSR-88D: description and application to an MCS. *Weather and Forecasting* **24**: 730–748, doi: 10.1175/2008WAF2222205.1.

Pinto J, Matthews JCG, Sarno GC. 2010. Stealth technology for wind turbines. *IET Radar Sonar Navig.* **4**: 126–133, doi: 10.1049/iet-rsn.2009.0031.

Rashid LS, Brown AK. 2011 'Radar cross-section analysis of wind turbine blades with radar absorbing materials'. In *Proceedings of the 2011 European Radar Conference (EuRAD)*, 12–14 October 2011. Manchester, UK, pp. 97–100.

RenewableUK. 2015. 'UK wind energy database (UKWED).' http://www.renewableuk.com/en/renewable-energy/wind-energy/uk-wind-energy-database/ (accessed 15 March 2016).

Rico-Ramirez MA, Cluckie ID. 2008. Classification of ground clutter and anomalous propagation using dual-polarization weather radar. *IEEE Trans. Geosci. Remote Sensing* **46**: 1892–1904, doi: 10.1109/TGRS.2008.916979.

Rico-Ramirez MA, Gonzalez-Ramirez E, Cluckie ID, Han D. 2009. Real-time monitoring of weather radar antenna pointing using digital terrain elevation and a Bayes clutter classifier. *Meteorol. Appl.* **16**: 227–236, doi: 10.1002/met.112.

Ryzhkov AV, Zrnic DS. 1998. Polarimetric rainfall estimation in the presence of anomalous propagation. *J. Atmos. Oceanic Technol.* **15**: 1320–1330, doi: 10.1175/1520-0426(1998)015<1320:PREITP>2.0.CO;2.

Schaefer JT. 1990. The critical success index as an indicator of warning skill. *Weather and Forecasting* **5**: 570–575, doi: 10.1175/1520-0434(1990)005<0570:TCSIAA>2.0.CO;2.

Schubel PJ, Crossley RJ. 2012. Wind turbine blade design. *Energies* **5**: 3425–3449, doi: 10.3390/en5093425.

Seo BC, Krajewski WF, Mishra KV. 2015. Using the new dual-polarimetric capability of WSR-88D to eliminate anomalous propagation and wind turbine effects in radar-rainfall. *Atmos. Res.* **153**: 296–309, doi: 10.1016/j.atmosres.2014.09.004.

Sinden G. 2007. Characteristics of the UK wind resource: Long-term patterns and relationship to electricity demand. *Energy Policy* **35**: 112–127, doi: 10.1016/j.enpol.2005.10.003.

Vogt RJ, Crum TD, Greenwood W, Ciardi EJ, Guenther RG. 2011. 'New criteria for evaluating wind turbine impacts on NEXRAD radars.' In *Proceedings of WINDPOWER 2011*. American Wind Energy Association: Anaheim, CA.

World Meteorological Organization (WMO). 2005. 'Impact of wind turbines on weather radars band'. *CBS/SG-RFC.* Doc 3.1(6), pp. 1–33.

World Meteorological Organization (WMO). 2010. *Commission for Instruments and Methods of Observation, Fifteenth Session.* WMO-No.1064. World Meteorological Organization: Geneva, Switzerland. http://www.wmo.int/pages/prog/www/CIMO/CIMO15-WMO1064/1064_en.pdf. (accessed 20 March 2016).